Full-Duplex DF Relaying With Parallel Hybrid FSO/RF Transmissions

MICHALIS P. NINOS (Member, IEEE), PRIYADARSHI MUKHERJEE (Member, IEEE), CONSTANTINOS PSOMAS (Senior Member, IEEE), AND IOANNIS KRIKIDIS (Fellow, IEEE)

Department of Electrical and Computer Engineering, University of Cyprus, Nicosia 1678, Cyprus

CORRESPONDING AUTHOR: M. P. NINOS (e-mail: ninos.michail@ucy.ac.cy)

ABSTRACT The ever-increasing demands for higher data rates in telecommunications networks, along with the significant benefits offered by wireless communications, have pushed the technological developments to new frontiers. Free-space optical (FSO) communications are among the technologies that can address these emerging demands, offering large and unregulated bandwidth. In addition, recent advances in radio frequency (RF) systems have enabled the development of in-band full-duplex (FD) radios with the employment of advanced self-interference cancelation techniques. Therefore, in this paper we study a robust FD relaying system comprised of parallel hybrid FSO/RF communication links, where the coordination of transmissions between the FSO/RF subsystems is carried out by the hard-switching protocol. The operation of the RF links is impaired by Nakagami-m fading, the residual self-interference due to the FD relaying operation, and the in-phase and quadrature-phase imbalance effect due to imperfect RF front-ends. As far as the FSO links are concerned, we consider the influence of the joint effects of atmospheric turbulence, beam wander and pointing errors. We first derive analytical closed-form expressions for the outage probability of both subsystems as well as for the overall FD relaying hybrid system. Then, asymptotic expressions are extracted for the outage performance in the high signal-to-noise ratio regime. The achievable outage diversity orders of both FSO and RF subsystems are determined, which provide significant insight into the design of such hybrid systems in a wide variety of operating conditions. Finally, the numerical results are presented using the derived outcomes, and significant conclusions are drawn about FD relaying hybrid systems.

INDEX TERMS Hybrid RF/FSO systems, full-duplex relaying, Nakagami-m fading, self-interference, IQ imbalance, atmospheric turbulence, beam wander, pointing errors, outage probability.

I. INTRODUCTION

WIRELESS communication systems have been at the forefront of many research efforts for over a century. As such, radio frequency (RF) communications have experienced tremendous development over the years. Nowadays, sophisticated RF systems have been developed aiming at high throughput performances with the highest possible spectral efficiency in accordance with the RF spectrum shortage and spectrum fees applied for its licensed frequency bands. Full-Duplex (FD) RF systems constitute a great example of

such developments [2]. In-band FD systems can transmit and receive at the same frequency band concurrently, offering an exceptional way of utilizing efficiently the time and frequency resources. However, FD operation can be hindered by unavoidable self-interference (SI) due to signal leakage from the transmit to the receive port. Advanced analog and digital SI cancelation techniques have been developed [3], which are capable of reducing very efficiently the impact of the SI. However, residual SI (RSI) signal power can still hamper the performance of such systems. A very promising

extension of FD operation is its incorporation into relaying architectures. Major performance benefits are offered by the utilization of FD relaying systems. Conventional RF relay architectures operate in half-duplex (HD) mode, i.e., transmit and receive either at different spectral bands or at different time slots (orthogonal channels) [4]. On the contrary, FD relaying provides very high spectral efficiency, where the relay node transmits and receives simultaneously at the same frequency band [4], [5], [6].

In addition, modern RF wireless transceivers incorporate up/down quadrature converters in order to accommodate the utilization of high spectral-efficient modulation schemes such as quadrature amplitude modulation (QAM) [7]. However, imperfections at the RF front-ends are inevitable, thus leading to performance limitations. Amplitude and phase mismatches between the in-phase (I) and quadrature-phase (Q) paths can arise due to imperfections in the local oscillator (LO) signal or any other stage involved in these paths, e.g., a low-pass filter [7], [8]. As a result, an imbalanced down-converted baseband signal can be corrupted by its image, thus leading to interference and signal-to-noise ratio (SNR) deterioration, an effect known as IQ imbalance (IQI) [9], [10].

On the other hand, the RF spectrum scarcity along with significant interference issues, due to the nature of the RF broadcast especially in the unlicensed bands, pose significant impediments for the implementation of reliable and efficient point-to-point RF links. Moreover, RF links experience the detrimental effects of multipath fading [11], [12]. As a viable alternative, free-space optical (FSO) communication systems operate in the unlicensed band of infrared frequencies. They offer larger and unregulated bandwidth, with FD capability, since FSO systems usually comprise one transmit and receive terminal [13]. Major challenges for wide terrestrial applications of FSO systems are their susceptibility to atmospheric effects, where turbulence-induced scintillation, fog attenuation and beam alignment disruptions degrade their performances [14], [15], [16]. As a consequence, FSO systems can reach distances up to some kilometres, by considering the imposed eye-safety constraints on the transmitted optical power. In order to overcome these issues, multi-hop relay architectures, with decode-and-forward (DF) or amplify-and-forward protocols, are studied for their distance coverage extension [17], [18].

Hybrid parallel FSO/RF systems are deemed as a viable and very promising solution in establishing high throughput and very reliable links [19]. The transmission characteristics of RF and FSO systems are complementary to each other [20]. Fog can break down the FSO beam transmission, while RF waves remain unaffected [21]. On the contrary, high rainfall hinders high-frequency RF transmission, while having lesser effect on FSO communication [22], [23]. Thus, the combination of these two technologies can create favorable conditions for setting up high-capacity and high-availability wireless connections [24], [25]. Moreover, parallel hybrid FSO/RF systems with the employment of

relay nodes, can offer extended coverage to longer distances [26]. Therefore, the implementation of a hybrid system with an FD RF relaying subsystem and a parallel dual-hop FSO subsystem offers highly efficient spectral use, extremely high availability and an increased wireless range.

Network topologies with parallel hybrid FSO/RF links and intermediate relay nodes have been extensively investigated in the literature so far. In [19], a source-destination hybrid FSO/millimeter wave RF link is discussed, wherein the hard-switching scheme is employed, by using single and dual FSO threshold implementations in Log-normal and Nakagami-m fading channels. In [25], the authors study a hybrid FSO/RF system with hard-switching operation and evaluate its performance in terms of the outage probability and bit error rate under the influence of Gamma-Gamma (GG) turbulence, pointing errors and Rician fading. In [26], the authors investigate optimal relay selection policies for the parallel hybrid RF/FSO relay channel with buffer-aided and non-buffer-aided relays. In [22], a switching-based cooperative DF relaying network with hybrid FSO/RF links and maximal ratio combining at the destination is investigated. Also, a DF relaying hybrid FSO/RF millimeter waves with selection combining is presented in [27], considering $\mathcal{M}$(alaga) turbulence with pointing errors and Weibull fading. In [24], the authors study a backhaul network with relay nodes connected with parallel hybrid FSO/RF links dealing with the problem of minimizing its cost while satisfying data rate and reliability constraints. In [28], they examine a wireless mesh network with parallel hybrid FSO/RF links between the relay nodes, with transmission power and optical beam-width adaptations in order to meet specified quality of service requirements such as throughput and end-to-end delay constraints. However, all the aforementioned works either do not discuss about the relaying operation or take into account HD relaying operation for the RF links. Motivated by the foregoing facts, in this paper for the first time, we examine the combination of an FD RF relaying subsystem with an FSO subsystem in a parallel hybrid relay topology.

More specifically, we investigate an FD DF relaying network, which consists of a source S, an FD DF relay R node and a destination D. The connection among the nodes is established with parallel hybrid FSO/RF links. For the routing of the information between the $S - R$ and $R - D$ links and the proper selection of the suitable subsystem for data transmission among the nodes, we consider the low-complexity hard-switching scheme [19], [21]. To the best of the authors knowledge, an FD DF relaying system with parallel hybrid FSO/RF links and hard-switching operation under the influence of Nakagami-m fading, RSI, IQI, atmospheric turbulence and pointing errors has not been investigated in the literature so far. Hence, we summarize the main contributions of this paper as follows.

- A detailed analysis of the system model is presented for an FD relaying setup with DF protocol consisted of parallel hybrid FSO/RF links. The considered dual-hop FD DF hybrid system operates under the hard-switching
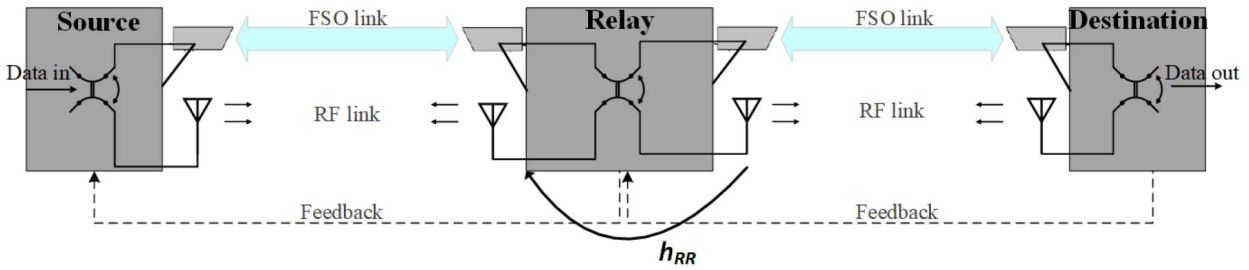
FIGURE 1. Block diagram of the considered full-duplex relaying communication system with parallel hybrid FSO/RF links under hard-switching operation.

scheme. We take into account the Nakagami-m fading, the RSI and IQI for the FD RF relaying subsystem, while for the FSO subsystem we consider the joint effects of GG turbulence, beam wander and pointing errors.

- We develop a novel channel model for the FSO links, where GG turbulence, beam wander and pointing errors are treated as three independent random variables. Analytical, closed-form expressions for the outage probability of the FSO and RF subsystems, as well as for the overall FD relaying hybrid system, are developed.

- Asymptotic expressions for the outage probability in the high signal-to-noise ratio (SNR) regime are derived for both subsystems. The outage diversity order of both FSO and RF subsystems is determined. In this way, we gain valuable insight into the design of such systems and we highlight the significance of the treatment of the FSO channel model as a product of three independent random variables.

- A variety of numerical results for the outage probability of the overall hybrid system is presented, taking into account the various effects that influence the FSO and RF subsystems. For the FD RF relaying subsystem, the effects of the RSI, the IQI and the generalized Nakagami-m fading are taken into account. Concerning the FSO subsystem, we investigate its performance under a variety of turbulence conditions with pointing errors, where the beam wander manifests itself at certain conditions. It is shown that proper beam parameter selection is essential under certain turbulence conditions. Eventually, all the derived results and the whole system model analysis, are verified by Monte Carlo simulations.

The rest of this paper is organized as follows. Section II describes the system model for the RF subsystem as well as the FSO subsystem. In Section III, we derive closed-form expressions for the outage probability of the RF and FSO subsystems and for the whole hybrid dual-hop system. In addition, asymptotic, tractable expressions in the high SNR regime are provided for both subsystems. Numerical and simulation results are presented in Section IV and the paper concludes with Section V.

Notation: $\mathbb{P}\{X\}$ and $\mathbb{E}\{X\}$ represent the probability and the expectation of X, respectively; $(\cdot)^*$ is the complex conjugate;

$\Gamma(\cdot)$, $\gamma(\cdot, \cdot)$, and $\Gamma(\cdot, \cdot)$ denote the complete, lower incomplete, and upper incomplete gamma function, respectively, $K_v(\cdot)$ is the modified Bessel function of the second kind and order v, $G_{p,q}^{m,n}(z|a_p; b_q)$ denotes the Meijer's G-function, and $\Phi(\cdot, \cdot; z)$, $_qF_p(a_q; b_p; z)$ represent the confluent and the generalized hypergeometric functions, respectively [29].

II. SYSTEM MODEL
A. TOPOLOGY
In this section, we elaborate on the system model for the individual FSO and RF subsystems, combined in a dual-hop FD hybrid set-up, as depicted in Figure 1. The system consists of a source S, an FD relay R node, employing the DF protocol, and a destination D. The source S transmits the information symbols either by using the FSO/RF subsystem according to the hard-switching scheme, with priority given to the larger bandwidth FSO link [19]. The hard-switching scheme is based upon the selection combining criterion [30], i.e., the activation of a subsystem is carried out with the selection of the highest SNR among them. Some notable algorithms for the implementation of the hard-switching protocol exist, which are the power hysteresis, the time hysteresis, the filtering method or a combination between them [21]. Besides the simplicity of the implementation of the hard-switching scheme, it requires one of the subsystems to be active at a time, compared to other combining approaches such as maximum ratio combining (MRC) or equal gain combining (EGC) [30]. In addition, an MRC or EGC would require both subsystems to be active and operating with the same data rate. Therefore, even if the FSO or RF subsystem is favorable for operation, it must be adapted to the performance capabilities of the other subsystem. Thus, an MRC or EGC can increase the reliability of the hybrid system, by concurrently exploiting two diversity branches, but diminishes the data throughput performance. Hence, we select the hard-switching scheme.

Thus, at a specific time slot, the subsystem of the $S-R$ link with the highest SNR is selected to transmit the information towards R, while the other remains idle. At R, the received signal is decoded and forwarded towards D. In case where the $S-R$ RF link is chosen for transmission, the detection process at R is influenced by the RSI due to the FD relaying operation and the IQI-impaired transmitted and received signal. On the contrary, if the $S-R$ FSO link is active, the

transmitted optical signal is corrupted by the atmospheric and misalignment effects, but is not affected by any type of interference. Note that the optical and the RF links do not interfere with each other, since they operate in completely different spectral bands. Also, for the RF subsystem, a direct line-of-sight $S-D$ link does not exist or any scattered signal is strongly attenuated and communication between them is established only with the aid of the FD relaying scheme [5], [26]. Consequently, the retrieved data at R is transmitted to D through the chosen FSO/RF link based again on the hard-switching operation. In case the $R-D$ RF link is activated for transmission, the RF transmitter at R and the destination RF receiver are impaired by the IQI effect. On the other hand, if the FSO $R-D$ link is selected for transmission, the optical signal experiences again the degradation atmospheric effects and reaches D, where is detected and decoded. In the following subsections, the mathematical representation models for both RF and FSO subsystems are presented.

B. RF SUBSYSTEM

For the RF links of the FD relaying RF subsystem, we employ the standard additive white Gaussian noise (AWGN) model. In addition, we take into account the effect of IQI at the transmitters (TXs) and receivers (RXs) of the RF nodes. The IQ mismatches constitute an inevitable effect in any RF quadrature up/down-converter, which arises primarily due to imperfections in the LO signal and secondly from any other transceiver stage. So, when we assume IQ mismatches, the IQI baseband signal is formulated as

$$x_{X,IQI}^{u/d}(t) = K_{1,X}^{u/d}x_X(t) + K_{2,X}^{u/d}(x_X(t))^* \quad (1)$$

with $x_X(t)$ being the desired signal and $(\cdot)^*$ denotes the image signal. The coefficients $K_{1,X}^{u/d}$, $K_{2,X}^{u/d}$ are defined as $K_{1,X}^{u/d} = 0.5(1 + \epsilon_X^{u/d}\exp(\pm j\phi_X^{u/d}))$ and $K_{2,X}^{u/d} = 1 - (K_{1,X}^{u/d})^*$, respectively, with the superscripts u/d signifying the up/down-conversion processes and the subscript $X \in (S, R, D)$. The parameters $\epsilon_X^{u/d}$, $\phi_X^{u/d}$ denote the amplitude and phase mismatches of the LO signals at the transceivers of each node [9], [10]. For instance, the mathematical representation of the IQI LO signal, used for downconversion, is described as

$$x_{LO,X} = \cos(\omega_{LO}t) - j\epsilon_X^d\sin\left(\omega_{LO}t + \phi_X^d\right)$$
$$= K_{1,X}^d\exp(-j\omega_{LO}t) + K_{2,X}^d\exp(j\omega_{LO}t), \quad (2)$$

where $\omega_{LO} = 2\pi f_{RF}$ with f_{RF} being the RF carrier frequency. Ideally, only the first term would have been present in the LO signal. The existence of the second term can lead to interference from the image signal after the downconversion process, which in turn can deteriorate the signal-to-interference-plus-noise ratio (SINR) of the desired signal [8], [9]. None of the existing image-reject receiver architectures can deal completely with the IQ mismatches arising in the quadrature converters [8]. The severity of IQ mismatches is quantified by the image rejection

ratio (IRR), defined as $IRR_X^{u/d} = |K_{1,X}^{u/d}/K_{2,X}^{u/d}|^2$, whose values, for typical front-end integrated circuits, ranges from 20 to 40 dB [8], [9], [10].

The source S, provided that the RF link is active, transmits an IQI-impaired symbol $x_{S,IQI}^u(t)$ with an average power $\mathbb{E}\{|x_S(t)|^2\} = P_t$. At the relay node R, considering front-end imperfections with IQI, the received signal is [31]

$$y_{R,RF}(t) = K_{1,R}^d h_{SR}x_{S,IQI}^u(t) + K_{2,R}^d\left(h_{SR}x_{S,IQI}^u(t)\right)^*$$
$$+ K_{1,R}^d h_{RR}x_{R,IQI}^u(t) + K_{2,R}^d\left(h_{RR}x_{R,IQI}^u(t)\right)^*$$
$$+ K_{1,R}^d n_R(t) + K_{2,R}^d(n_R(t))^*, \quad (3)$$

where $x_{R,IQI}^u(t)$ is the IQI-impaired transmitted signal from R again with an average transmitted power $\mathbb{E}\{|x_R(t)|^2\} = P_t$. The channel coefficient h_{SR} is equal to $h_{SR} = \sqrt{\hat{h}_{SR}}\tilde{h}_{SR}$, where the individual terms are described as [11], [12], [26]

$$\hat{h}_k = \left[\frac{c\sqrt{G_{TX}G_{RX}}}{4\pi f_{RF}L_k}\right]^2 \text{ and } \left|\tilde{h}_k\right| \sim \text{Nakagami}(m_k, \Omega_k) \quad (4)$$

with $k \in (SR, RD)$, where $c = 3 \times 10^8$ m/s is the speed of light, G_{TX}, G_{RX} are the transceiver antenna gains, L_k is the link distance. It is worthy to note that, in this work, we consider frequencies below 10 GHz, for which the rainfall does not have a significant impact.[1] Moreover, we assume the Nakagami-m model which has been proved a very accurate model for multipath propagation, encompassing as special cases the one-sided Gaussian ($m = 1/2$), Rayleigh ($m = 1$) and Rice distributions [11]. The channel coefficient h_{RR} and the term $n_R(t)$ correspond to the RSI and the AWGN at R, respectively, which are circularly symmetric complex Gaussian random variables with zero mean and variance σ_{RR}^2 and σ_n^2, respectively, i.e., $h_{RR} \sim \mathcal{CN}(0, \sigma_{RR}^2)$ and $n_R(t) \sim \mathcal{CN}(0, \sigma_n^2)$. For simplification reasons, we introduce the notations

$$\lambda_{RR} \triangleq 2\sigma_{RR}^2 \quad \text{and} \quad \hat{\Omega}_k \triangleq \hat{h}_k\Omega_k.$$

The received signal at D, considering IQI at the relay TX and the destination RX, is

$$y_{D,RF}(t) = K_{1,D}^d h_{RD}x_{R,IQI}^u(t) + K_{2,D}^d\left(h_{RD}x_{R,IQI}^u(t)\right)^*$$
$$+ K_{1,D}^d n_D(t) + K_{2,D}^d(n_D(t))^*, \quad (5)$$

with $h_{RD} = \sqrt{\hat{h}_{RD}}\tilde{h}_{RD}$ described similarly as in (4) and $n_D(t) \sim \mathcal{CN}(0, \sigma_n^2)$.

Next, taking into account the aforementioned analysis, we proceed with the evaluation of the SINRs for the $S-R$ and $R-D$ RF links, i.e., $\gamma_{RF,SR}$ and $\gamma_{RF,RD}$, respectively. More

---

1. Based on [23], we use the aR^b relation to calculate the specific attenuation due to the rainfall, where R is the rainfall rate in mm/hr and a, b are the coefficients which are calculated by the Laws and Parsons Distribution for high rainfall (LP$_H$). For $f_{RF} = 6$ GHz the values for a and b for rain temperature at 0^oC are equal to 1.99×10^{-3} and 1.285, respectively. By assuming a strong rainfall with R = 25.4 mm/hr, the specific attenuation is calculated as 0.13 dB/km. Thus, for a 2 km propagation distance, the total loss is 0.26 dB, which can be considered negligible.

precisely, for the $S - R$ RF link, considering the RSI and IQI impairments, $\gamma_{RF,SR}$ is formulated as

$$\gamma_{RF,SR} = \frac{S_1 P_t}{(I_1 + I_2)P_t + \left(\left|K_{1,R}^d\right|^2 + \left|K_{2,R}^d\right|^2\right)\sigma_n^2}, \quad (6)$$

where S_1, I_1 and I_2 are equal to

$$S_1 = \left|K_{1,R}^d K_{1,S}^u h_{SR} + K_{2,R}^d \left(K_{2,S}^u h_{SR}\right)^*\right|^2,$$

$$I_1 = \left|K_{1,R}^d K_{2,S}^u h_{SR} + K_{2,R}^d \left(K_{1,S}^u h_{SR}\right)^*\right|^2, \quad \text{and}$$

$$I_2 = \left|K_{1,R}^d K_{1,R}^u h_{RR} + K_{2,R}^d \left(K_{2,R}^u h_{RR}\right)^*\right|^2$$
$$+ \left|K_{1,R}^d K_{2,R}^u h_{RR} + K_{2,R}^d \left(K_{1,R}^u h_{RR}\right)^*\right|^2.$$

For scenarios with a perfect matching between the IQ branches, the IQI effect becomes negligible, i.e., $K_{1,X}^{u/d} = 1$ and $K_{2,X}^{u/d} = 0$. As a result, the terms I_1, I_2 become $I_1 = |h_{RR}|^2$, $I_2 = 0$ and hence, (6) simplifies to

$$\gamma_{RF,SR} = \frac{P_t |h_{SR}|^2}{P_t |h_{RR}|^2 + \sigma_n^2}. \quad (7)$$

With regards to the $R - D$ RF link, the transmitted IQI-impaired symbol from R reaches D, having propagated through the Nakagami-m distributed fading channel. The demodulation stage at the RX of D is also influenced by the IQI effect. Hence, for the case of TX/RX IQI-impaired nodes, the SINR of the $R - D$ RF link is [10, Eq. (33)]

$$\gamma_{RF,RD} = \frac{|\vartheta_{11}|^2 + |\vartheta_{22}|^2}{|\vartheta_{12}|^2 + |\vartheta_{21}|^2 + \left(|K_{1,D}^d|^2 + |K_{2,D}^d|^2\right)\frac{1}{\gamma_{id,RD}}}, \quad (8)$$

where $\vartheta_{11} = K_{1,D}^d K_{1,R}^u$, $\vartheta_{12} = K_{1,D}^d K_{2,R}^u$, $\vartheta_{21} = K_{2,D}^d (K_{1,R}^u)^*$, $\vartheta_{22} = K_{2,D}^d (K_{2,R}^u)^*$, and $\gamma_{id,RD} = P_t |h_{RD}|^2/\sigma_n^2$ denoting the ideal SNR in the absence of IQI. When the IQI is negligible, we obtain $\vartheta_{11} = 1$, $\vartheta_{12} = 0$, $\vartheta_{21} = 0$, and $\vartheta_{22} = 0$, respectively, and as a result, (8) simplifies to $\gamma_{RF,RD} = \gamma_{id,RD}$.

C. FSO SUBSYSTEM
In case that the FSO link is active, S activates the optical terminal and sends the information signal towards R. Intensity modulation with direct detection (IM/DD) mode [32] is employed and the AWGN model is considered for all the sources of noise entailed in the FSO links, e.g., shot noise, thermal noise etc. The optical signal is emitted by the source S and propagates through the atmospheric channel, wherein experiences all the aggravating effects related to the atmospheric medium, such as atmospheric turbulence, beam wander and pointing errors [14], [15], [16]. After the detection of the optical signal at R, the signal is re-encoded and transmitted from R to D by using the FSO/RF link, as it has already been described. The $S - R$ and $R - D$ FSO links can be characterized as identical since no interference issues take place at R due to the narrow optical beams employed [26].

Thus, the received signal at the input of the relay R or the destination D photodetector (PD) is described as [33]

$$y_{FSO,k}(t) = I_k s(t) + n_{opt}(t), \quad (9)$$

where $s(t)$ is the transmitted information symbol from each node with an average transmitted optical power $\mathbb{E}\{|s(t)|^2\} = P_0$, I_k, $k \in (SR, RD)$ is the total real-valued instantaneous channel coefficient of each hop, and n_{opt} corresponds to the AWGN of the optical link $n_{opt} \sim \mathcal{N}(0, \sigma_{n,opt}^2)$. The total channel coefficient, I_k, can be represented as a product of three independent random variables, i.e., $I_k = I_{t,k} I_{b,k} I_{p,k}$, where $I_{t,k}$ corresponds to the atmospheric turbulence effect, $I_{b,k}$ to the beam wander, and $I_{p,k}$ to the pointing errors and geometrical loss. The instantaneous electrical SNR at the PD receiver output of each individual k-th FSO link is [32]

$$\gamma_{FSO,k} = \frac{(\rho_k P_0 I_k)^2}{\sigma_{n,opt}^2}, \quad (10)$$

and the average electrical SNR is defined as [32]

$$\overline{\gamma}_{FSO,k} = \frac{(\rho_k P_0 \mathbb{E}\{I_k\})^2}{\sigma_{n,opt}^2}, \quad (11)$$

with ρ_k being the PD responsivity in A/W. Due to the independence between the channel coefficients, we obtain $\mathbb{E}\{I_k\} = \mathbb{E}\{I_{t,k}\}\mathbb{E}\{I_{p,k}\}\mathbb{E}\{I_{b,k}\}$.

It is well-known that the probability density function (PDF) of the GG distribution accurately models the irradiance fluctuations ranging from weak to strong turbulence conditions. Its PDF is given as [34], [35]

$$f_{I_{t,k}}(I_{t,k}) = \frac{2}{\Gamma(a_k)\Gamma(b_k)I_{t,k}} \left(\frac{a_k b_k I_{t,k}}{I_{l,k}}\right)^{\frac{a_k + b_k}{2}}$$
$$\times K_{a_k - b_k}\left(2\sqrt{\frac{a_k b_k I_{t,k}}{I_{l,k}}}\right). \quad (12)$$

The term $I_{l,k}$ represents the deterministic attenuation of the optical signal due to scattering and absorption and is calculated by the Beer-Lambert law [36]. The expected value of $I_{t,k}$ is equal to $\mathbb{E}\{I_{t,k}\} = I_{l,k}$ [34]. The parameters a_k, b_k of the GG distribution, for plane wave propagation, are given as [37]

$$a_k = \left[\exp\left(\frac{0.49\sigma_{R,k}^2}{\left(1 + 0.65d_k^2 + 1.11\sigma_{R,k}^{12/5}\right)^{7/6}}\right) - 1\right]^{-1},$$

$$b_k = \left[\exp\left(\frac{0.51\sigma_{R,k}^2\left(1 + 0.69\sigma_{R,k}^{12/5}\right)^{-5/6}}{\left(1 + 0.9d_k^2 + 0.62d_k^2\sigma_{R,k}^{12/5}\right)^{5/6}}\right) - 1\right]^{-1}, \quad (13)$$

where $\sigma_{R,k}^2$ is the Rytov variance, calculated as $\sigma_{R,k}^2 = 1.23C_{n,k}^2 \kappa^{7/6} L_k^{11/6}$ with $C_{n,k}^2$ denoting the refractive index structure parameter, which usually takes values in the range $10^{-17} - 10^{-13} \text{m}^{-2/3}$ for weak up to strong turbulence conditions. The parameter d_k is defined as $d_k = 0.5D_R\sqrt{\kappa L_k^{-1}}$ with

D_R denoting the diameter of each PD aperture of the dual-hop FSO subsystem, L_k being the link distance of the $S-R$, $R-D$ links and $\kappa = 2\pi/\lambda$ being the optical wavenumber.

The PDF of the pointing errors effect, due to terminal movements, is given as [15]

$$f_{I_{p,k}}(I_{p,k}) = \frac{\xi_k^2}{A_{0,k}^{\xi_k^2}} I_{p,k}^{\xi_k^2-1}, 0 \leq I_{p,k} \leq A_{0,k}, \qquad (14)$$

with the parameters ξ_k, $A_{0,k}$ being defined as $\xi_k = W_{z,eq}/\sigma_{s,k}$, $A_{0,k} = [\text{erf}(\upsilon)]^2$, with $\sigma_{s,k}$ being the standard deviation of the beam's radial displacement, $\upsilon_k = \sqrt{2\pi}D_R/4W_{z,k}$ and $\text{erf}(\cdot)$ is the error function. The equivalent beam radius is calculated as $W_{z,eq,k} = \sqrt{\pi}\text{erf}(\upsilon_k)W_{z,k}^2/2\upsilon_k\exp(-\upsilon_k^2)$ and is linked with the beam radius $W_{z,k}$ on the RX plane at distance L_k [15]. Its value is calculated as $W_{z,k} = W_k\sqrt{1 + 1.63\sigma_{R,k}^{12/5}\Lambda_k}$, where $W_k = W_0\sqrt{\Theta_{0,k}^2 + \Lambda_{0,k}^2}$ and $\Lambda_k = \frac{\Lambda_{0,k}}{\Theta_{0,k}^2 + \Lambda_{0,k}^2}$, with $\Theta_{0,k}$, $\Lambda_{0,k}$ being the input plane beam parameters defined as $\Theta_{0,k} = 1 - \frac{L_k}{F_0}$, $\Lambda_{0,k} = \frac{2L_k}{\kappa W_0}$ [14]. The parameter W_0 corresponds to the beam radius at each TX of the FSO subsystem and F_0 is the phase front radius of curvature, which for the case of a collimated beam $F_0 \rightarrow \infty$ [14]. The expected value of $I_{p,k}$ is $\mathbb{E}\{I_{p,k}\} = A_{0,k}\xi_k^2(1 + \xi_k^2)^{-1}$ [32, Eq. (23)].

Additional irradiance fluctuations can be inflicted by the beam wander-induced jitter due to large-scale atmospheric turbulence [38]. The authors in [39] propose a beta distribution in order to characterize the effect of beam motion due to atmospheric turbulence, which is given as

$$f_{I_{b,k}}(I_{b,k}) = \beta_{w,k}I_{b,k}^{\beta_{w,k}-1}, 0 \leq I_{b,k} \leq 1, \qquad (15)$$

where the parameter $\beta_{w,k}$ is evaluated as [40]

$$\beta_{w,k} = \sqrt{1 + \frac{1 + \sigma_I^2}{34.29\left(\frac{\Lambda_k L_k}{kr_{0,k}^2}\right)^{5/6}\left(\frac{\sigma_{pe,k}}{W_{z,k}}\right)^2}} - 1, \qquad (16)$$

and is linked with the scintillation index $\sigma_I^2 = \frac{1}{a_k} + \frac{1}{b_k} + \frac{1}{a_kb_k}$ [35]. The parameter $\sigma_{pe,k}^2$ refers to the jitter-induced pointing error variance due to beam wander and for the case of a collimated beam is calculated as [38, Eq. (14)], with C_r being a scaling constant selected equal to 1.5π for a horizontal propagation path [16]. The parameter $r_{0,k} = (0.16C_{n,k}^2\kappa^2L_k)^{-3/5}$ is the Fried parameter and the expected value of $I_{b,k}$ is calculated as $\mathbb{E}\{I_{b,k}\} = \int_0^1 xf_{I_{b,k}}(x)dx = \frac{\beta_{w,k}}{\beta_{w,k}+1}$.

III. OUTAGE PROBABILITY ANALYSIS
In this section, we investigate the outage probability of the individual RF and FSO subsystems and for the FD DF relaying hybrid FSO/RF system. Firstly, we derive the outage probability of the RF subsystem for the $S-R$ and $R-D$ links and then for the corresponding FSO links. Lastly, we

TABLE 1. The parameters A_1, B_1 and B_2 involved in (17), (18).

$A_1 = $	$\left\|K_{1,R}^d K_{1,S}^u\right\|^2 + \left\|K_{2,R}^d K_{2,S}^{u,*}\right\|^2$
$B_1 = $	$\left\|K_{1,R}^d K_{2,S}^u\right\|^2 + \left\|K_{2,R}^d K_{1,S}^{u,*}\right\|^2$
$B_2 = $	$\|K_{1,R}^d K_{1,R}^u\|^2 + \left\|K_{2,R}^d K_{2,R}^{u,*}\right\|^2 + \left\|K_{1,R}^d K_{2,R}^u\right\|^2 + \left\|K_{2,R}^d K_{1,R}^{u,*}\right\|^2$

combine the derived outcomes to obtain the outage probability of the FD relaying hybrid system with parallel FSO/RF links.

A. RF SUBSYSTEM OUTAGE PROBABILITY
On condition that the RF link is active, an outage occurs for the $S-R$ link when the instantaneous $\gamma_{RF,SR}$ falls below a predefined threshold $\gamma_{th,RF} = 2^{R_{th,RF}} - 1$ with R_{th} being the threshold achievable rate in bits per channel use (BPCU). Considering that $\gamma_{RF,SR}$ of (6) depends on the Nakagami-m fading and the RSI, we formulate the following theorem for the $S-R$ outage probability estimation.

Theorem 1: The outage probability of the $S-R$ RF link, taking into account that $\gamma_{RF,SR}$ is a function of the channel gains $|h_{SR}|^2$ and $|h_{RR}|^2$, is given by

$$P_{out,RF,SR} = \frac{1}{\Gamma(m_{SR})}$$
$$\times \left[\gamma\left(m_{SR}, \frac{m_{SR}\gamma_{th,RF}}{\hat{\Omega}_{SR}(P_t/\sigma_n^2)}\right) + \exp\left(\frac{\left|K_{1,R}^d\right|^2 + \left|K_{2,R}^d\right|^2}{\lambda_{RR}B_2(P_t/\sigma_n^2)}\right) \right.$$
$$\times \left(1 + \frac{\hat{\Omega}_{SR}\left(\frac{A_1}{\gamma_{th,RF}} - B_1\right)}{m_{SR}\lambda_{RR}B_2}\right)^{-m_{SR}}$$
$$\left. \times \Gamma\left(m_{SR}, \left(1 + \frac{\hat{\Omega}_{SR}\left(\frac{A_1}{\gamma_{th,RF}} - B_1\right)}{m_{SR}\lambda_{RR}B_2}\right)\frac{m_{SR}\gamma_{th,RF}}{\hat{\Omega}_{SR}(P_t/\sigma_n^2)}\right) \right]$$
$$\qquad (17)$$

where $\gamma_{th,RF} = 2^{R_{th,RF}} - 1$ and the parameters A_1, B_1 and B_2 are shown in Table 1.

Proof: See Appendix A. ∎

The derived, exact expression of (17), for the $S-R$ outage probability, is quite cumbersome and does not provide direct insight into the $S-R$ RF subsystem behavior. In order to get a more simplified expression, we derive an asymptotic approximation in the following corollary, when $\frac{P_t}{\sigma_n^2} \rightarrow \infty$.

Corollary 1: When the ratio $\frac{P_t}{\sigma_n^2} \rightarrow \infty$, the outage probability for the $S-R$ RF link is asymptotically approximated as

$$\lim_{\frac{P_t}{\sigma_n^2} \rightarrow \infty} P_{out,RF,SR} = \left(1 + \frac{\hat{\Omega}_{SR}\left(\frac{A_1}{\gamma_{th,RF}} - B_1\right)}{m_{SR}\lambda_{RR}B_2}\right)^{-m_{SR}}. \qquad (18)$$

Proof: See Appendix B. ∎

From the tractable approximation of (18), we observe that the $S-R$ outage performance converges to an outage floor, dependent on the Nakagami parameters (m_{SR}, Ω_{SR}), the RSI,

the IQ mismatches. Thus, the $S - R$ outage diversity order is zero. Likewise, for the $R - D$ RF link outage probability evaluation, the following theorem is formulated.

Theorem 2: The outage probability for the $R-D$ RF link is

$$P_{out,RF,RD} = \frac{1}{\Gamma(m_{RD})}$$

$$\times \gamma\left(m_{RD}, \frac{m_{RD}}{\widehat{\Omega}_{RD}(P_t/\sigma_n^2)} \frac{|K_{1,D}^d|^2 + |K_{2,D}^d|^2}{\frac{|\vartheta_{11}|^2+|\vartheta_{22}|^2}{\gamma_{th}} - (|\vartheta_{12}|^2 + |\vartheta_{21}|^2)}\right) \tag{19}$$

Proof: See Appendix C. ∎

In addition, for the sake of completeness, we provide a tractable high SNR regime-based asymptotic approximation for the outage probability of the $R - D$ RF link as follows.

Corollary 2: When the ratio $\frac{P_t}{\sigma_n^2} \rightarrow \infty$, the outage probability for the $R - D$ RF link is given by

$$\lim_{\frac{P_t}{\sigma_n^2} \rightarrow \infty} P_{out,RF,RD} = \frac{1}{\Gamma(m_{RD}+1)}$$

$$\times \left(\frac{m_{RD}}{\widehat{\Omega}_{RD}(P_t/\sigma_n^2)} \frac{|K_{1,D}^d|^2 + |K_{2,D}^d|^2}{\frac{|\vartheta_{11}|^2+|\vartheta_{22}|^2}{\gamma_{th,RF}} - (|\vartheta_{12}|^2 + |\vartheta_{21}|^2)}\right)^{m_{RD}} \tag{20}$$

It is observed that the $R - D$ outage diversity order of the RF link is m_{RD}. However, the outage behavior of the total FD DF relaying RF subsystem at the high $\frac{P_t}{\sigma_n^2}$ regime is determined by the minimum diversity order and thus we conclude to the following remark.

Remark 1: The outage diversity order of the RF FD DF relaying subsystem is determined by the minimum diversity order between the $S - R$ and $R - D$ RF links. Therefore, the outage diversity order of the RF subsystem is zero (error floor).

B. FSO SUBSYSTEM OUTAGE PROBABILITY

As it is already stated in Section II-C, since no interference occurs at R or from any other ambient source, the FSO subsystem consists of identical $S - R$, $R - D$ links. Thus, the outage probability of the individual FSO links can be evaluated by having the cumulative distribution function (CDF) $F_{\gamma_{FSO,k}}(x)$ of the instantaneous $\gamma_{FSO,k}$. Since the total channel coefficient I_k is a product of three independent random variables, i.e., $I_k = I_{t,k}I_{b,k}I_{p,k}$, we conclude to the following theorem for the outage probability estimation of the individual $S - R$ and $R - D$ FSO links.

Theorem 3: The outage probability for each individual FSO link, incorporating the GG distribution, the pointing errors effect, and the beam wander-induced jitter, is

$$P_{out,FSO,k} = F_{\gamma_{FSO,k}}(\gamma_{th,FSO}) = \frac{\beta_{w,k}\xi_k^2}{\Gamma(a_k)\Gamma(b_k)}$$

$$\times G_{3,5}^{4,1}\left(\frac{a_k b_k \mathbb{E}\{I_k\}}{A_{0,k}I_{l,k}}\sqrt{\frac{\gamma_{th,FSO}}{\overline{\gamma}_{FSO,k}}}\Bigg| \begin{matrix}1, \beta_{w,k}+1, \xi_k^2+1\\ \xi_k^2, \beta_{w,k}, a_k, b_k, 0\end{matrix}\right), \tag{21}$$

where $\gamma_{th,FSO} = 2^{R_{th,FSO}} - 1$.

Proof: See Appendix D. ∎

In addition to the closed-form expression of (21), we provide an asymptotic analysis, which is valid when $\overline{\gamma}_{FSO,k} \rightarrow \infty$. In the following corollary, we define the outage diversity order of the considered FSO system model and valuable engineering insight into the FSO subsystem behavior at high $\overline{\gamma}_{FSO,k}$ is obtained.

Corollary 3: The outage diversity order of the FSO link impaired by GG atmospheric turbulence, beam wander, and pointing errors is evaluated as

$$\mathcal{O}_d = \frac{\min(a_k, b_k, \beta_{w,k}, \xi_k^2)}{2}. \tag{22}$$

Proof: See Appendix E. ∎

C. HYBRID DUAL-HOP FSO/RF OUTAGE PROBABILITY

The overall outage probability of the dual-hop hybrid system can be written as [41]

$$P_{out,tot} = P_{out,SR} + (1 - P_{out,SR})P_{out,RD}, \tag{23}$$

where $P_{out,SR}$, denotes the outage probability of the hybrid FSO/RF $S - R$ link and $P_{out,RD}$ denotes the corresponding outage probability of the $R - D$ link. Based on the hard-switching operation, the outage probability of each individual hop, is [19], [30]

$$P_{out,k} = P_{out,RF,k}P_{out,FSO,k} \tag{24}$$

Thus, based on (24) we can deduce that the outage probability of the FD DF relaying hybrid system composed of parallel hybrid FSO/RF links, under hard-switching operation, is

$$P_{out,tot} = P_{out,RF,SR}P_{out,FSO,SR}$$
$$+ (1 - P_{out,RF,SR}P_{out,FSO,SR})$$
$$\times P_{out,RF,RD}P_{out,FSO,RD}, \tag{25}$$

where $P_{out,RF,SR}$ is replaced by the expressions either of Theorem 1 or Corollary 1 for the exact or asymptotic case, $P_{out,RF,RD}$ from the expressions of Theorem 2 or Corollary 2, while $P_{out,FSO,SR}$ and $P_{out,FSO,RD}$ are given by the Theorem 3 or (42), shown at the top of the p. 13 for the exact or the asymptotic case, respectively.

IV. NUMERICAL RESULTS

In this section, we present the numerical results based on the aforementioned analysis and derivations. For the illustrated results, we assume different conditions among the $S - R$ and $R - D$ links for both FSO and RF subsystems, characterized by the following relations for the corresponding fading conditions $m_{RD} = m_{SR} + 3$, $\Omega_{RD} = \Omega_{SR} + 5\,\text{dB}$ and $C_{n,RD}^2 = C_{n,SR}^2/3$. In addition, all the presented results are accompanied by Monte Carlo simulations using 10^6 realizations, which corroborate the analysis conducted in the previous sections. Unless otherwise stated, the values used for the various parameters, of the FSO and RF subsystems, are contained in Table 2.

TABLE 2. Parameter values for the RF and FSO subsystems.

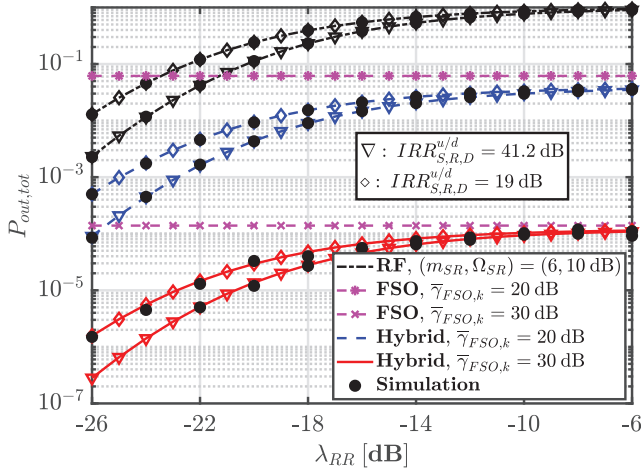| RF links		FSO links	
Parameter	Value	Parameter	Value
f_{RF}	6 GHz	λ	1.55 um
G_{TX}, G_{RX}	50 dBi	D_R	10 cm
$R_{th,RF}$	4 BPCU	$R_{th,FSO}$	4 BPCU
λ_{RR}	$(-26, -16), (-20, -10)$ dB	W_0	4 cm
L_{SR}, L_{RD}	2 km	L_{SR}, L_{RD}	2 km
P_t/σ_n^2	60 dB	F_0	∞ [38]
$IRR_{S,R,D}^{u/d}$	$19, 25.4, 41.2$ dB	$\sigma_{s,k}$	1 cm
(m_{SR}, Ω_{SR})	$(3, 7$ dB$), (6, 10$ dB$)$	$C_{n,SR}^2$	6×10^{-14} m$^{-2/3}$

FIGURE 2. Outage probability versus λ_{RR}.

Figure 2 illustrates the outage probability results for the FD DF relaying hybrid system as a function of the mean value of the RSI effect λ_{RR}. We take into account weak and strong IQI impact on the RF subsystem front-ends at all the three nodes (S, R, D). For the RF links, we assume a moderate multipath fading environment, while for the FSO links we assume two cases of operation with two values for $\overline{\gamma}_{FSO,k}$ under strong turbulence conditions. From the derived plots, we deduce the performance improvement of the outage probability $P_{out,tot}$ of the hybrid system. Compared to the cases when the dual-hop system is exclusively composed of FSO or RF links, $P_{out,tot}$ reaches acceptable values below 10^{-3}. Specifically, when $\overline{\gamma}_{FSO,k} = 20$ dB, $P_{out,tot}$ reaches values below 10^{-3} for a range of values for λ_{RR} between -26 to -22 or -24 dB, depending on the IQI level. Consequently, when $\overline{\gamma}_{FSO,k} = 30$ dB, a significant performance improvement is observed. Note that $P_{out,tot}$ lies on the order of 10^{-7} for $\lambda_{RR} = -26$ dB and reaches values up to 10^{-4} when $\lambda_{RR} = -6$ dB. Furthermore, we also observe the impact of the IQI on the outage performance. As it is shown, the influence of the IQI becomes evident when the RSI is kept at minimum levels. Otherwise, for $\lambda_{RR} \geq -12$ dB, we cannot observe significant difference due to the IQI, and the performance is determined mostly by the RSI, the multipath fading, the atmospheric turbulence and $\overline{\gamma}_{FSO,k}$. This clearly indicates the severity of the RSI and the importance to keep it at the minimum possible levels. Eventually, we can infer that the FSO links can counterbalance any performance degradation inflicted by the FD
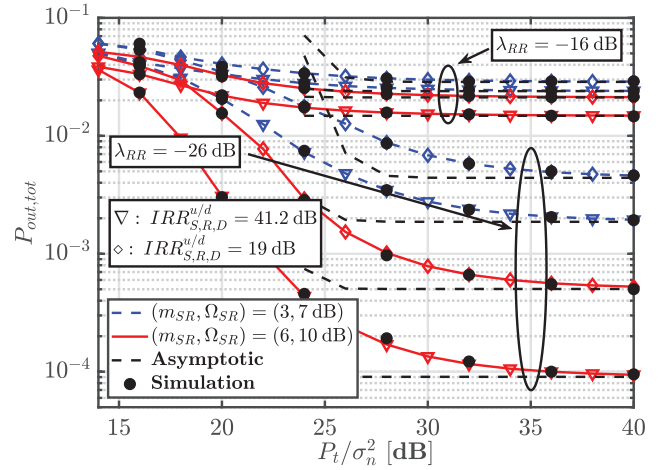

FIGURE 3. Outage probability versus P_t/σ_n^2; $\overline{\gamma}_{FSO,k} = 20$ dB.

relaying operation of the RF links in case that high $\overline{\gamma}_{FSO,k}$ can be attained.

Next, in Figure 3, we present the outage probability performance for the dual-hop FD hybrid system as a function of the ratio $\frac{P_t}{\sigma_n^2}$, along with the asymptotic ones in the high $\frac{P_t}{\sigma_n^2}$ regime. The IQ mismatches and the RSI are taken into account, with weak and strong influence. As far as the wireless RF channels are concerned, two different conditions are employed, corresponding to strong and weak multipath fading, respectively. For the FSO links, we assume strong atmospheric turbulence and misalignment fading, with fixed $\overline{\gamma}_{FSO,k} = 20$ dB. For the most favorable conditions, with $(m_{SR}, \Omega_{SR}) = (6, 10$ dB$)$, $\lambda_{RR} = -26$ dB and $\frac{P_t}{\sigma_n^2} = 40$ dB, $P_{out,tot}$ is on the order of 9×10^{-5} with strong IQ mismatches, whereas for weak IQI is at 5×10^{-4}. In addition, we can clearly notice the impact of multipath fading on the outage performance. For the case where $(m_{SR}, \Omega_{SR}) = (3, 7$ dB$)$ and $\lambda_{RR} = -26$ dB, we observe that the outage probability increases to 2×10^{-3} or 5×10^{-3} for weak or strong IQ mismatches, respectively. On the other hand, we observe again the detrimental impact of the RSI on the FD relaying hybrid FSO/RF system. For $\lambda_{RR} = -16$ dB, the outage probability is on the order of 10^{-2}, irrespective of the influence of multipath fading, RSI and IQI. Interestingly, the results indicate that the performance aggravation due to IQI becomes more evident when weak multipath fading and weak RSI are considered. Moreover, the availability of the FD relaying hybrid system under strong RSI, can be increased with higher $\overline{\gamma}_{FSO,k}$ values for the FSO subsystem, i.e., $\overline{\gamma}_{FSO,k} > 20$ dB and better RF wireless propagation conditions. Regarding the asymptotic results, we notice the tightness that provide in the high $\frac{P_t}{\sigma_n^2}$ regime compared to the exact expressions, while corroborating the remark that the outage performance reaches an error floor.

In Figure 4, outage probability results are shown versus the $\overline{\gamma}_{FSO,k}$ along with the asymptotic ones in the high $\overline{\gamma}_{FSO,k}$ regime. For the FSO links, we consider two cases for the turbulence strength with moderate and very strong
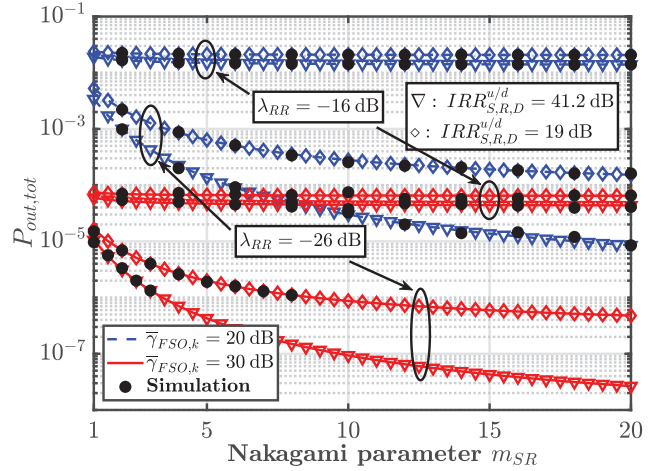
TABLE 3. The outage diversity order $\mathcal{O}_d$ for the FSO links for various turbulence conditions.

Turbulence conditions	$C_{n,k}^2 \left(\text{m}^{-2/3} \right)$	Dominant term	Exact Eq. (21)	Deviation (%)	$\mathcal{O}_d$
Weak	4×10^{-15}	$\mathcal{J}_2 = 3.61 \times 10^{-24}$	3.61×10^{-24}	0	$\frac{\beta_{w,k}}{2} = 5.5$
Moderate	1×10^{-14}	$\mathcal{J}_2 = 3.97 \times 10^{-18}$	3.97×10^{-18}	0	$\frac{\beta_{w,k}}{2} = 4.28$
Strong	6×10^{-14}	$\mathcal{J}_3 = 1.81 \times 10^{-13}$	1.67×10^{-13}	8.4	$\frac{a_k}{2} = 3.52$
Very strong	1×10^{-13}	$\mathcal{J}_3 = 2.62 \times 10^{-13}$	2.48×10^{-13}	6.1	$\frac{a_k}{2} = 3.39$
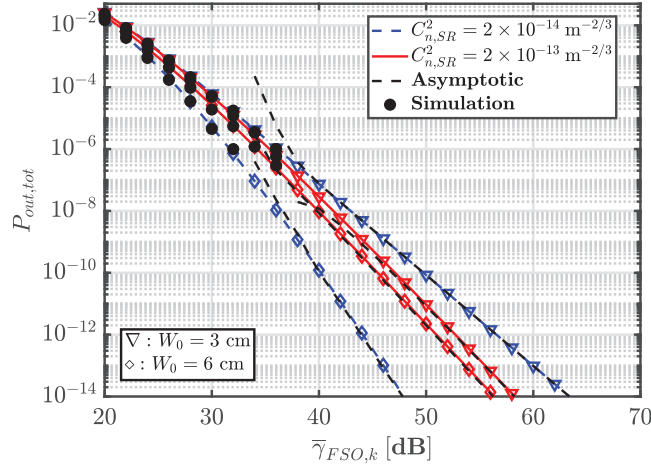
FIGURE 4. Outage probability as a function of $\overline{\gamma}_{FSO,k}$; $(m_{SR}, \Omega_{SR}) = (3, 7 \text{ dB})$, $\lambda_{RR} = -10 \text{ dB}$, $IRR_{S,R,D}^{u/d} = 25.4 \text{ dB}$.

FIGURE 5. Outage probability versus Nakagami parameter m_{SR}; $\Omega_{SR} = 10 \text{ dB}$.

turbulence conditions. Moreover, we select two values for W_0, corresponding to narrow and wide beamwidths. We can observe that as $\overline{\gamma}_{FSO,k}$ tends to values higher than 30 dB, the outage probability of the dual-hop FD hybrid link is improved essentially with attained values at 10^{-4} and smaller. In addition, we must point out the differences that arise due to the selection of different beam radius sizes W_0 at the transmitters of each node. Specifically, for the moderate turbulence case, at high $\overline{\gamma}_{FSO,k}$ values, we can observe the $\overline{\gamma}_{FSO,k}$ gain achieved with the employment of $W_0 = 6$ cm. On the order of 10^{-9} for $P_{out,tot}$, the $\overline{\gamma}_{FSO,k}$ gain is roughly 8 dB compared to the case with $W_0 = 3$ cm. On the other hand, when very strong turbulence conditions are considered, the corresponding achievable $\overline{\gamma}_{FSO,k}$ gain is not so high. In conclusion, it is revealed that the beam parameters can play a significant role under certain turbulence conditions, where beam wander-induced jitter can influence the FSO link performance. As far as the asymptotic results are concerned, we observe the perfect matching that offer compared to the exact results, especially when $\overline{\gamma}_{FSO,k} > 40$ dB.

Capitalizing on the above-mentioned observations for the FSO links, in Table 3, we present a variety of results for the outage diversity order under various turbulence conditions. In this table we include the various turbulence conditions characterized by the $C_{n,k}^2$ parameter, the dominant terms from the asymptotic expression of (42) and the exact outage probability from (21). Next, the percentage deviation of the dominant term value from the exact outage probability is evaluated and the corresponding values of the outage diversity orders

are presented for the various conditions. For these results, we consider $R_{th,FSO} = 5$ BPCU, while the rest parameters are drawn from Table 2, along with $\overline{\gamma}_{FSO,k} = 60$ dB. It is noticed from Corollary 3, that the outage diversity order, for the considered FSO links, interchanges with respect to the turbulence conditions. Specifically, under weak and moderate atmospheric turbulence, the $\mathcal{O}_d$ is determined by the parameter of the beam wander-induced jitter $\beta_{w,k}$. On the other hand, for strong and very strong turbulence conditions, the $\mathcal{O}_d$ is specified by the large-scale turbulence parameter a_k of the GG distribution. The derived results verify the theory, which dictates that under weak turbulence conditions the beam wander can be quite evident, whereas in strong turbulence conditions beam wander is less severe and the beam is divided into a multitude of smaller spots. Therefore, we can deduce that from weak to moderate turbulence conditions, the beam wander effect must be taken seriously into consideration, with proper beam parameter selection when high throughput systems are designed, i.e., in the high $\overline{\gamma}_{FSO,k}$ regime. In strong turbulence conditions, refractive and diffractive phenomena contribute essentially to the turbulence-induced scintillations. As a consequence, proper link design must be carried out, taking into account the link distance and the beam parameters in order to overcome the atmospherically-induced effects and achieve high performance FSO links. It is worth pointing out that the $\mathcal{O}_d$ can be determined also by the ξ_k parameter of pointing errors, particularly when sway of the FSO terminals becomes prominent, a case investigated in Figure 7.

In Figure 5, the outage probability performance is depicted as a function of the Nakagami fading parameter m_{SR}. For
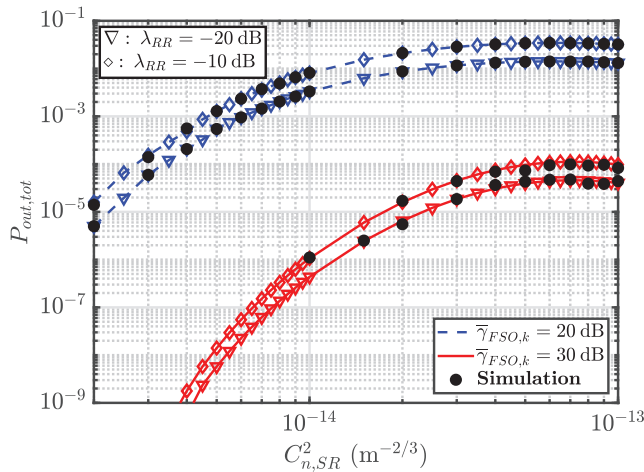
FIGURE 6. Outage probability versus $C^2_{n,SR}$; $(m_{SR}, \Omega_{SR}) = (3, 7\,\text{dB})$, $IRR^{u/d}_{S,R,D} = 25.4\,\text{dB}$.

FIGURE 7. Outage probability versus $\sigma_{s,k}$; $\overline{\gamma}_{FSO,k} = 30\,\text{dB}$, $\lambda_{RR} = -20\,\text{dB}$, $IRR^{u/d}_{S,R,D} = 25.4\,\text{dB}$.

the illustrated results, we assume strong turbulence conditions for the FSO links, with two values for $\overline{\gamma}_{FSO,k}$. For the FD RF relaying subsystem we assume two cases for the RSI, corresponding to weak and strong influence of the effect. From the derived plots, we observe the dependence of the outage performance of the FD relaying hybrid system on the $\overline{\gamma}_{FSO,k}$. For the higher $\overline{\gamma}_{FSO,k}$ value, we observe a performance improvement of three orders of magnitude for all the illustrated cases. Concerning the RSI impact, we see again its detrimental impact on the FD relaying hybrid system. Specifically, when $\overline{\gamma}_{FSO,k} = 20\,\text{dB}$ and $\lambda_{RR} = -16\,\text{dB}$, the outage performance of the hybrid system is on the order of 10^{-2}, irrespective of the IQI level. Lastly, we can clearly notice the impact of the IQI effect on the hybrid system's outage performance, when the RSI is weak and at high values of the Nakagami parameter, i.e., when multipath fading vanishes.

Figure 6 shows the outage probability versus $C^2_{n,SR}$. We consider two cases of operation for the FSO links, characterized by the $\overline{\gamma}_{FSO,k}$. For the FD RF relaying subsystem, we consider strong multipath fading and IQI. We observe that in the weak turbulence regime, the outage performance, for the case of $\overline{\gamma}_{FSO,k} = 20\,\text{dB}$, lies in acceptable levels. When $C^2_{n,SR} \geq 6 \times 10^{-15}\,\text{m}^{-2/3}$ (i.e., from moderate to strong turbulence), the outage probability exceeds the limit of 10^{-3} for both cases of strong and weak RSI. On the contrary, when $\overline{\gamma}_{FSO,k} = 30\,\text{dB}$, the outage performance remains at acceptable levels from weak to very strong turbulence conditions even when $\lambda_{RR} = -10\,\text{dB}$.

Eventually, Figure 7 depicts the outage probability versus the $\sigma_{s,k}$ parameter of the pointing errors. For the FSO links, we consider fixed $\overline{\gamma}_{FSO,k} = 30\,\text{dB}$ and two cases for the beam radius and the turbulence strength as well. For the FD RF relaying subsystem we assume two cases for the RF propagation environment, with strong and weak multipath fading, along with IQI influence. As it is shown, the beam size plays a major role in the overall performance of the hybrid system. At a first glance, we observe an unexpected phenomenon,
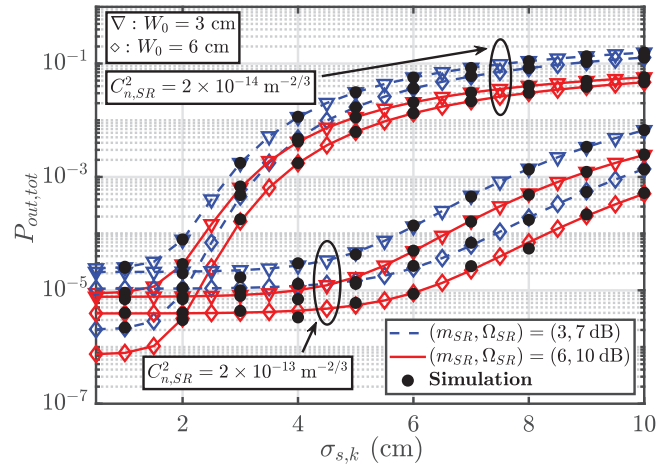
where for the case of moderate turbulence conditions and narrow beam size we obtain the worst case performance, compared to the corresponding ones with strong turbulence, especially when $\sigma_{s,k} > 2\,\text{cm}$. This is mainly attributed to optical turbulence; the beam spreading due to turbulence acts in a beneficial way, compensating for the beam displacements due to pointing errors. On the other hand, in the moderate regime, the beam spreading is smaller and thus the irradiance fluctuations become immense as the spatial jitter increases, having a significant effect on the outage performance of the hybrid system. Concerning the RF wireless environment, we can see the performance improvement between the two considered cases, under both weak and strong atmospheric turbulence conditions. In general, under moderate turbulence, $P_{out,tot}$ achieves values below the limit of 10^{-3} across the range of $\sigma_{s,k} \leq 3.5\,\text{cm}$, whereas for the strong turbulence case, a spatial jitter of $\sigma_{s,k} \leq 8\,\text{cm}$ is tolerable.

V. CONCLUSION

In this work, we investigate an FD DF relaying communication system with parallel hybrid FSO/RF links. The FD RF relaying subsystem is impaired by the RSI and the IQI effect at the front-ends of each node and the FSO subsystem operates under the joint influence of GG atmospheric turbulence, beam wander and pointing errors. Under these assumptions, the outage performance of the dual-hop FD DF hybrid FSO/RF system is analyzed. Novel, tractable closed-form expressions for the outage probability are derived along with their asymptotic approximations in the high SNR regime. The asymptotic approximation results unveiled the vital characteristics of operation of the hybrid communication system, and significant insight into the design of FD DF relaying systems with parallel hybrid FSO/RF links is provided. Specifically, we showed that for weak turbulence conditions, the beam wander affects the FSO link performance and proper selection of beam parameters can counterbalance its impact on the FD relaying hybrid system. On the contrary, we observe that in strong turbulence conditions the beam parameter selection

does not play a significant role and the performance of the hybrid system is degraded essentially under such conditions. Moreover, for the FD RF relaying subsystem we demonstrate that its outage probability performance reaches an outage floor, which is strongly dependent on the RSI, the Nakagami parameters and the IQ mismatch. We conclude that major performance limitations are primarily caused by the atmospheric turbulence, Nakagami-m fading, and RSI. The impact of the IQI becomes evident in scenarios of weak RSI and finally, the pointing errors influence the performance when the spatial jitter increases substantially.

APPENDIX A
PROOF OF THEOREM 1
Firstly, we introduce some approximations for (6) of $\gamma_{RF,SR}$. Knowing that the inequality $|\alpha|^2 + |\beta|^2 \gg 2\mathbb{R}(\alpha\beta^*)$ holds, i.e., $|\alpha + \beta|^2 \approx |\alpha|^2 + |\beta|^2$, we obtain

$$S_1 \approx \left|K_{1,R}^d K_{1,S}^u h_{SR}\right|^2 + \left|K_{2,R}^d\left(K_{2,S}^u h_{SR}\right)^*\right|^2 \approx A_1 |h_{SR}|^2,$$

$$I_1 \approx \left|K_{1,R}^d K_{2,S}^u h_{SR}\right|^2 + \left|K_{2,R}^d\left(K_{1,S}^u h_{SR}\right)^*\right|^2 \approx B_1 |h_{SR}|^2,$$

and

$$I_2 \approx \left|K_{1,R}^d K_{1,R}^u h_{RR}\right|^2 + \left|K_{2,R}^d\left(K_{2,R}^u h_{RR}\right)^*\right|^2$$
$$+ \left|K_{1,R}^d K_{2,R}^u h_{RR}\right|^2 + \left|K_{2,R}^d\left(K_{1,R}^u h_{RR}\right)^*\right|^2 \approx B_2 |h_{RR}|^2,$$

where the parameters A_1, B_1 and B_2 are shown in Table 1.

Consequently, we evaluate the conditional probability $\mathbb{P}\{\gamma_{RF,SR} \leq \gamma_{th}||h_{SR}|^2\}$, given that $|h_{SR}|^2$ is known. Since $h_{RR} \sim \mathcal{CN}(0, \sigma_{RR}^2)$, $|h_{RR}|^2$ is exponentially distributed with mean value λ_{RR}, i.e., $f_{|h_{RR}|^2}(x) = \frac{1}{\lambda_{RR}}\exp(-\frac{x}{\lambda_{RR}})$ for $x \geq 0$, the $\mathbb{P}\{\gamma_{RF,SR} \leq \gamma_{th}||h_{SR}|^2\}$ is obtained by replacing the $\gamma_{RF,SR}$ from (6), as depicted in (26), shown at the bottom of the page. Similarly, due to the fact that $|\tilde{h}_{SR}| \sim \text{Nakagami}(m_{SR}, \Omega_{SR})$, $|h_{SR}|^2$ is gamma distributed as $f_{|h_{SR}|^2}(x) = \frac{1}{\Gamma(m_{SR})}(\frac{m_{SR}}{\hat{\Omega}_{SR}})^{m_{SR}} x^{m_{SR}-1}\exp(-\frac{m_{SR}x}{\hat{\Omega}_{SR}})$ for $x \geq 0$. Thus, the outage probability of the $S-R$ RF link is calculated by using the integral formulae of (27) shown at the bottom of the page, concluding to the corresponding closed-form expression.

APPENDIX B
PROOF OF COROLLARY 1
For the asymptotic approximation of (17), when $\frac{P_t}{\sigma_n^2} \to \infty$, we use the equality $\gamma(m, z) = m^{-1}z^m\Phi(m, 1 + m; -z)$ [29, Eq. (6.5.12)]. By knowing that $\Phi(\cdot, \cdot; z) \to 1$ when $z \to 0$, (17) is approximated as

$$\lim_{\frac{P_t}{\sigma_n^2}\to\infty} P_{out,RF,SR} = \frac{1}{\Gamma(m_{SR})}\left[\frac{1}{m_{SR}}\left(\frac{m_{SR}\gamma_{th,RF}}{\hat{\Omega}_{SR}(P_t/\sigma_n^2)}\right)^{m_{SR}}\right.$$
$$\left.+ \left(1 + \frac{\hat{\Omega}_{SR}\left(\frac{A_1}{\gamma_{th}} - B_1\right)}{m_{SR}\lambda_{RR}B_2}\right)^{-m_{SR}}\left(\Gamma(m_{SR})\right.\right.$$

$$\mathbb{P}\left\{\gamma_{RF,SR} \leq \gamma_{th}\middle| |h_{SR}|^2\right\} = \mathbb{P}\left\{\left(\frac{A_1}{\gamma_{th}B_2} - \frac{B_1}{B_2}\right)|h_{SR}|^2 - \frac{\left|K_{1,R}^d\right|^2 + \left|K_{2,R}^d\right|^2}{B_2(P_t/\sigma_n^2)} \leq |h_{RR}|^2\middle| |h_{SR}|^2\right\}$$

$$= \begin{cases} \exp\left[-\frac{1}{\lambda_{RR}}\left(\left(\frac{A_1}{\gamma_{th}B_2} - \frac{B_1}{B_2}\right)|h_{SR}|^2 - \frac{\left|K_{1,R}^d\right|^2 + \left|K_{2,R}^d\right|^2}{B_2(P_t/\sigma_n^2)}\right)\right], & |h_{SR}|^2 > \gamma_{th}/(P_t/\sigma_n^2) \\ 1, & |h_{SR}|^2 \leq \gamma_{th}/(P_t/\sigma_n^2) \end{cases} \quad (26)$$

$$P_{out,RF,SR} = \int_0^\infty \mathbb{P}\left\{\left(\frac{A_1}{\gamma_{th}B_2} - \frac{B_1}{B_2}\right)x - \frac{\left|K_{1,R}^d\right|^2 + \left|K_{2,R}^d\right|^2}{B_2(P_t/\sigma_n^2)} \leq |h_{RR}|^2\middle| |h_{SR}|^2\right\}f_{|h_{SR}|^2}(x)dx$$

$$= \int_0^{\gamma_{th}/\frac{P_t}{\sigma_n^2}} \frac{1}{\Gamma(m_{SR})}\left(\frac{m_{SR}}{\hat{\Omega}_{SR}}\right)^{m_{SR}} x^{m_{SR}-1}\exp\left(-\frac{m_{SR}x}{\hat{\Omega}_{SR}}\right)dx$$

$$+ \int_{\gamma_{th}/\frac{P_t}{\sigma_n^2}}^\infty \exp\left[-\frac{1}{\lambda_{RR}}\left(\left(\frac{A_1}{\gamma_{th}B_2} - \frac{B_1}{B_2}\right)x - \frac{\left|K_{1,R}^d\right|^2 + \left|K_{2,R}^d\right|^2}{B_2(P_t/\sigma_n^2)}\right)\right]\frac{1}{\Gamma(m_{SR})}\left(\frac{m_{SR}}{\hat{\Omega}_{SR}}\right)^{m_{SR}} x^{m_{SR}-1}\exp\left(-\frac{m_{SR}x}{\hat{\Omega}_{SR}}\right)dx$$

$$= \frac{1}{\Gamma(m_{SR})}\left[\gamma\left(m_{SR}, \frac{m_{SR}\gamma_{th}}{\hat{\Omega}_{SR}(P_t/\sigma_n^2)}\right) + \exp\left(\frac{\left|K_{1,R}^d\right|^2 + \left|K_{2,R}^d\right|^2}{\lambda_{RR}B_2(P_t/\sigma_n^2)}\right)\left(1 + \frac{\hat{\Omega}_{SR}\left(\frac{A_1}{\gamma_{th}} - B_1\right)}{m_{SR}\lambda_{RR}B_2}\right)^{-m_{SR}}\right.$$

$$\left.\times \Gamma\left(m_{SR}, \left(1 + \frac{\hat{\Omega}_{SR}\left(\frac{A_1}{\gamma_{th}} - B_1\right)}{m_{SR}\lambda_{RR}B_2}\right)\frac{m_{SR}\gamma_{th}}{\hat{\Omega}_{SR}(P_t/\sigma_n^2)}\right)\right] \quad (27)$$

$$-\frac{1}{m_{SR}}\left(\left(1+\frac{\hat{\Omega}_{SR}\left(\frac{A_1}{\gamma_{th}}-B_1\right)}{m_{SR}\lambda_{RR}B_2}\right)\frac{m_{SR}\gamma_{th}}{\hat{\Omega}_{SR}\left(P_t/\sigma_n^2\right)}\right)^{m_{SR}}\Bigg)\Bigg]$$

$$=\left(1+\frac{\hat{\Omega}_{SR}\left(\frac{A_1}{\gamma_{th}}-B_1\right)}{m_{SR}\lambda_{RR}B_2}\right)^{-m_{SR}} \tag{28}$$

and we obtain (18).

APPENDIX C
PROOF OF THEOREM 2

By using (8), the outage probability of the $R-D$ RF link, i.e., $P_{out,RF,RD}=\mathbb{P}\{\gamma_{RF,RD}\leq\gamma_{th}\}$ is expressed as

$$P_{out,RF,RD}=\mathbb{P}\left\{\frac{|K_{1,D}^d|^2+|K_{2,D}^d|^2}{\frac{|\vartheta_{11}|^2+|\vartheta_{22}|^2}{\gamma_{th}}-\left(|\vartheta_{12}|^2+|\vartheta_{21}|^2\right)}\geq\gamma_{id,RD}\right\}. \tag{29}$$

We require the CDF of $\gamma_{id,RD}$ to calculate the $P_{out,RF,RD}$. Knowing that $\gamma_{id,RD}$ is a function of $|h_{RD}|^2$, the CDF of $\gamma_{id,RD}$ is obtained as [42]

$$F_{\gamma_{id,RD}}(x)=\frac{\gamma\left(m_{RD},\frac{mx}{\hat{\Omega}_{RD}(P_t/\sigma_n^2)}\right)}{\Gamma(m_{RD})} \tag{30}$$

So, the outage probability of the $R-D$ RF link is

$$P_{out,RF,RD}=F_{\gamma_{id,RD}}\left(\frac{|K_{1,D}^d|^2+|K_{2,D}^d|^2}{\frac{|\vartheta_{11}|^2+|\vartheta_{22}|^2}{\gamma_{th}}-\left(|\vartheta_{12}|^2+|\vartheta_{21}|^2\right)}\right). \tag{31}$$

By replacing the argument of (31) into (30), we obtain the closed-form expression of $P_{out,RF,RD}$ as presented in (19).

APPENDIX D
PROOF OF THEOREM 3

In [43], the Mellin Transform (MT) is utilized to study the distribution of products of independent random variables. So, for the case of the channel state of FSO links, which is a product of three independent random variables, $I_k=I_{t,k}I_{b,k}I_{p,k}$, we apply the following multiplicative property

$$\mathcal{M}\left(f_{I_k}(I_k)|s\right)=\mathcal{M}\left(f_{I_{t,k}}(I_{t,k})|s\right)\mathcal{M}\left(f_{I_{p,k}}(I_{p,k})|s\right)$$
$$\times\mathcal{M}\left(f_{I_{b,k}}(I_{b,k})|s\right), \tag{32}$$

where $\mathcal{M}(f_x(x)|s)=\int_0^\infty f_x(x)x^{s-1}dx, x\geq 0$ denotes the MT of the function $f_x(x)$ and s is a complex number. The MT of the GG distribution is derived as

$$\mathcal{M}\left(f_{I_{t,k}}(I_{t,k})|s\right)=\frac{\Gamma(s+a_k-1)\Gamma(s+b_k-1)}{\Gamma(a_k)\Gamma(b_k)\left(\frac{a_kb_k}{I_{l,k}}\right)^{s-1}}. \tag{33}$$

The MT for the distribution of the pointing errors, given in (14), is calculated as

$$\mathcal{M}\left(f_{I_{p,k}}(I_{p,k})|s\right)=\frac{\xi_k^2}{A_{0,k}^{1-s}}\frac{\Gamma\left(s+\xi_k^2-1\right)}{\Gamma\left(s+\xi_k^2\right)}, \tag{34}$$

while from (15), the MT for the PDF of the beam wander effect, which is a beta distribution, is [43]

$$\mathcal{M}\left(f_{I_{b,k}}(I_{b,k})|s\right)=\beta_{w,k}\frac{\Gamma\left(s+\beta_{w,k}-1\right)}{\Gamma\left(s+\beta_{w,k}\right)}. \tag{35}$$

By the use of the multiplicative property of (32), we obtain

$$\mathcal{M}\left(f_{I_k}(I_k)|s\right)=\frac{\beta_{w,k}\xi_k^2}{\Gamma(a_k)\Gamma(b_k)}\frac{\Gamma(s+a_k-1)}{\Gamma\left(s+\xi_k^2\right)}$$
$$\times\frac{\Gamma(s+b_k-1)\Gamma\left(s+\xi_k^2-1\right)}{\Gamma\left(s+\beta_{w,k}\right)}$$
$$\times\Gamma\left(s+\beta_{w,k}-1\right)\left(\frac{A_{0,k}I_{l,k}}{a_kb_k}\right)^{s-1}. \tag{36}$$

Taking the inverse MT of $\mathcal{M}(f_{I_k}(I_k)|s)$ as $f_{I_k}(I_k)=\frac{1}{2\pi j}\int_{c-j\infty}^{c+j\infty}\mathcal{M}(f_{I_k}(I_k)|s)I_k^{-s}ds$, we obtain the PDF of the total channel coefficient I_k as

$$f_{I_k}(I_k)=\frac{\beta_{w,k}\xi_k^2a_kb_k}{A_{0,k}I_{l,k}\Gamma(a_k)\Gamma(b_k)}\frac{1}{2\pi j}$$
$$\times\int_{c-j\infty}^{c+j\infty}\frac{\Gamma(s+a_k-1)\Gamma(s+b_k-1)}{\Gamma\left(s+\xi_k^2\right)}$$
$$\times\frac{\Gamma\left(s+\xi_k^2-1\right)\Gamma\left(s+\beta_{w,k}-1\right)}{\Gamma\left(s+\beta_{w,k}\right)}\left(\frac{A_{0,k}I_{l,k}}{a_kb_kI_k}\right)^s ds, \tag{37}$$

where using [44, Eq. (6.422.19)], we derive

$$f_{I_k}(I_k)=\frac{\beta_{w,k}\xi_k^2a_kb_k}{A_{0,k}I_{l,k}\Gamma(a_k)\Gamma(b_k)}$$
$$\times G_{4,2}^{0,4}\left(\frac{A_{0,k}I_{l,k}}{a_kb_kI_k}\left|\begin{matrix}2-\xi_k^2,2-\beta_{w,k},2-a_k,2-b_k\\1-\beta_{w,k},1-\xi_k^2\end{matrix}\right.\right). \tag{38}$$

Accordingly, by applying [44, Eq. (9.31.2)], we obtain

$$f_{I_k}(I_k)=\frac{\beta_{w,k}\xi_k^2a_kb_k}{A_{0,k}I_{l,k}\Gamma(a_k)\Gamma(b_k)}$$
$$\times G_{2,4}^{4,0}\left(\frac{a_kb_kI_k}{A_{0,k}I_{l,k}}\left|\begin{matrix}\beta_{w,k},\xi_k^2\\\xi_k^2-1,\beta_{w,k}-1,a_k-1,b_k-1\end{matrix}\right.\right). \tag{39}$$

The corresponding CDF is derived as [45, Eq. (26)]

$$F_{I_k}(I_k)=\frac{\beta_{w,k}\xi_k^2}{\Gamma(a_k)\Gamma(b_k)}$$
$$\times G_{3,5}^{4,1}\left(\frac{a_kb_kI_k}{A_{0,k}I_{l,k}}\left|\begin{matrix}1,\beta_{w,k}+1,\xi_k^2+1\\\xi_k^2,\beta_{w,k},a_k,b_k,0\end{matrix}\right.\right). \tag{40}$$

Combining (10) and (11), we can express the instantaneous $\gamma_{FSO,k}$ as $\gamma_{FSO,k}=\frac{\bar{\gamma}_{FSO,k}}{(\mathbb{E}\{I_k\})^2}I_k^2$. The CDF of $\gamma_{FSO,k}$ is derived following a simple random variable transformation, concluding to

$$F_{\gamma_{FSO,k}}(x)=\frac{\beta_{w,k}\xi_k^2}{\Gamma(a_k)\Gamma(b_k)}$$
$$\times G_{3,5}^{4,1}\left(\frac{a_kb_k\mathbb{E}\{I_k\}}{A_{0,k}I_{l,k}}\sqrt{\frac{x}{\bar{\gamma}_{FSO,k}}}\left|\begin{matrix}1,\beta_{w,k}+1,\xi_k^2+1\\\xi_k^2,\beta_{w,k},a_k,b_k,0\end{matrix}\right.\right). \tag{41}$$

Thus, the outage probability of the FSO links can be calculated as presented in Theorem 3.

$$\lim_{\overline{\gamma}_{FSO,k} \to \infty} F_{\gamma_{FSO,k}}(x) = \underbrace{\frac{\beta_{w,k}\Gamma(a_k - \xi_k^2)\Gamma(b_k - \xi_k^2)z^{\xi_k^2}}{(\beta_{w,k} - \xi_k^2)\Gamma(a_k)\Gamma(b_k)}}_{\mathcal{J}_1} + \underbrace{\frac{\xi_k^2\Gamma(a_k - \beta_{w,k})\Gamma(b_k - \beta_{w,k})z^{\beta_{w,k}}}{(\xi_k^2 - \beta_{w,k})\Gamma(a_k)\Gamma(b_k)}}_{\mathcal{J}_2}$$
$$+ \underbrace{\frac{\beta_{w,k}\xi_k^2\Gamma(b_k - a_k)z^{a_k}}{(\beta_{w,k} - a_k)(\xi_k^2 - a_k)\Gamma(b_k)\Gamma(1 + a_k)}}_{\mathcal{J}_3} + \underbrace{\frac{\beta_{w,k}\xi_k^2\Gamma(a_k - b_k)z^{b_k}}{(\beta_{w,k} - b_k)(\xi_k^2 - b_k)\Gamma(a_k)\Gamma(1 + b_k)}}_{\mathcal{J}_4} \qquad (42)$$

APPENDIX E
PROOF OF COROLLARY 3

In order to derive an asymptotic approximation of (21), we utilize the expansion formula for the Meijer's G-function in terms of the generalized hypergeometric function $_qF_p(a_q; b_p; z)$ as given in [44, Eq. (9.303)], where $z = \frac{a_k b_k \mathbb{E}\{I_k\}}{A_{0,k}I_{l,k}}\sqrt{\frac{x}{\overline{\gamma}_{FSO,k}}}$. On condition that $\overline{\gamma}_{FSO,k} \to \infty$, i.e., $z \to 0$, then $_qF_p(a_q; b_p; z) \to 1$ and (21) is approximated as depicted in (42), where asymptotically the outage probability behaves as $P_{out,FSO,k} \approx (\mathcal{O}_c\overline{\gamma}_{FSO,k})^{-\mathcal{O}_d}$, with $\mathcal{O}_c$ and $\mathcal{O}_d$ denoting the coding gain and the outage diversity order, respectively [5]. Thus, we observe that the outage diversity order varies between four parameters which are $\frac{a_k}{2}$, $\frac{b_k}{2}$, $\frac{\beta_{w,k}}{2}$ and $\frac{\xi_k^2}{2}$, concluding to Corollary 3.

REFERENCES

[1] M. P. Ninos, P. Mukherjee, C. Psomas, and I. Krikidis, "Dual-hop full-duplex DF relay channel with parallel hybrid RF/FSO links," in *Proc. IEEE GLOBECOM*, Madrid, Spain, Dec. 2021, pp. 1–6.

[2] M. Chung, M. S. Sim, J. Kim, D. K. Kim, and C.-B. Chae, "Prototyping real-time full duplex radios," *IEEE Commun. Mag.*, vol. 53, no. 9, pp. 56–63, Sep. 2015.

[3] M. S. Sim, M. Chung, D. Kim, J. Chung, D. K. Kim, and C.-B. Chae, "Nonlinear self-interference cancellation for full-duplex radios: From link-level and system-level performance perspectives," *IEEE Commun. Mag.*, vol. 55, no. 9, pp. 158–167, Sep. 2017.

[4] T. Riihonen, S. Werner, and R. Wichman, "Hybrid full-duplex/half-duplex relaying with transmit power adaptation," *IEEE Trans. Wireless Commun.*, vol. 10, no. 9, pp. 3074–3085, Sep. 2011.

[5] I. Krikidis, H. A. Suraweera, P. J. Smith, and C. Yuen, "Full-duplex relay selection for amplify-and-forward cooperative networks," *IEEE Trans. Wireless Commun.*, vol. 11, no. 12, pp. 4381–4393, Dec. 2012.

[6] H. A. Suraweera, I. Krikidis, G. Zheng, C. Yuen, and P. J. Smith, "Low-complexity end-to-end performance optimization in MIMO full-duplex relay systems," *IEEE Trans. Wireless Commun.*, vol. 13, no. 2, pp. 913–927, Feb. 2014.

[7] S. Mirabbasi and K. Martin, "Classical and modern receiver architectures," *IEEE Commun. Mag.*, vol. 38, no. 11, pp. 132–139, Nov. 2000.

[8] B. Razavi, "Transceiver architectures," in *RF Microelectronics*. Upper Saddle River, NJ, USA: Prentice Hall, 2012, pp. 155–254.

[9] L. Anttila, M. Valkama, and M. Renfors, "Circularity-based I/Q imbalance compensation in wideband direct-conversion receivers," *IEEE Trans. Veh. Technol.*, vol. 57, no. 4, pp. 2099–2113, Jul. 2008.

[10] A. A. Boulogeorgos, P. C. Sofotasios, B. Selim, S. Muhaidat, G. K. Karagiannidis, and M. Valkama, "Effects of RF impairments in communications over cascaded fading channels," *IEEE Trans. Veh. Technol.*, vol. 65, no. 11, pp. 8878–8894, Nov. 2016.

[11] M.-S. Alouini and M. K. Simon, "Performance analysis of coherent equal gain combining over Nakagami-*m* fading channels," *IEEE Trans. Veh. Technol.*, vol. 50, no. 6, pp. 1449–1463, Nov. 2001.

[12] Y. Zhang, J. Zhang, L. Yang, B. Ai, and M.-S. Alouini, "On the performance of dual-hop systems over mixed FSO/mmWave fading channels," *IEEE Open J. Commun. Soc.*, vol. 1, pp. 477–489, 2020.

[13] H. Willebrand and B. Ghuman, *Free Space Optics: Enabling Connectivity in Today's Networks*. Indianapolis, IN, USA: SAMS Publ., 2001.

[14] L. C. Andrews and R. L. Phillips, *Laser Beam Propagation Through Random Media*. Bellingham, WA, USA: SPIE, 2005.

[15] A. A. Farid and S. Hranilovic, "Outage capacity optimization for free-space optical links with pointing errors," *J. Lightw. Technol.*, vol. 25, no. 7, pp. 1702–1710, Jul. 2007.

[16] J. Recolons, L. C. Andrews, and R. L. Phillips, "Analysis of beam wander effects for a horizontal-path propagating Gaussian-beam wave: Focused beam case," *Opt. Eng.*, vol. 46, no. 8, Aug. 2007, Art. no. 086002.

[17] K. P. Peppas, A. N. Stassinakis, H. E. Nistazakis, and G. S. Tombras, "Capacity analysis of dual amplify-and-forward relayed free-space optical communication systems over turbulence channels with pointing errors," *IEEE/OSA J. Opt. Commun. Netw.*, vol. 5, no. 9, pp. 1032–1042, Sep. 2013.

[18] H. E. Nistazakis, M. P. Ninos, A. D. Tsigopoulos, D. A. Zervos, and G. S. Tombras, "Performance study of terrestrial multi-hop OFDM FSO communication systems with pointing errors over turbulence channels," *J. Modern Opt.*, vol. 63, no. 14, pp. 1403–1413, Jun. 2016.

[19] M. Usman, H. Yang, and M.-S. Alouini, "Practical switching-based hybrid FSO/RF transmission and its performance analysis," *IEEE Photon. J.*, vol. 6, no. 5, pp. 1–13, Oct. 2014.

[20] I. I. Kim and E. J. Korevaar, "Availability of free-space optics (FSO) and hybrid FSO/RF systems," in *Optical Wireless Communications IV*, vol. 4530. Denver, CO, USA: SPIE, Nov. 2001, pp. 84–95.

[21] F. Nadeem, B. Geiger, E. Leitgeb, S. Muhammad, M. Loeschnig, and G. Kandus, "Comparison of link selection algorithms for free space optics/radio frequency hybrid network," *IET Commun.*, vol. 5, no. 18, pp. 2751–2759, Dec. 2011.

[22] S. Sharma, A. S. Madhukumar, and R. Swaminathan, "Switching-based cooperative decode-and-forward relaying for hybrid FSO/RF networks," *IEEE/OSA J. Opt. Commun. Netw.*, vol. 11, no. 6, pp. 267–281, Jun. 2019.

[23] R. Olsen, D. Rogers, and D. Hodge, "The aR^b relation in the calculation of rain attenuation," *IEEE Trans. Antennas Propag.*, vol. 26, no. 2, pp. 318–329, Mar. 1978.

[24] A. Douik, H. Dahrouj, T. Y. Al-Naffouri, and M.-S. Alouini, "Hybrid radio/free-space optical design for next generation backhaul systems," *IEEE Trans. Commun.*, vol. 64, no. 6, pp. 2563–2577, Jun. 2016.

[25] A. Touati, A. Abdaoui, F. Touati, M. Uysal, and A. Bouallegue, "On the effects of combined atmospheric fading and misalignment on the hybrid FSO/RF transmission," *IEEE/OSA J. Opt. Commun. Netw.*, vol. 8, no. 10, pp. 715–725, Oct. 2016.

[26] M. Najafi, V. Jamali, and R. Schober, "Optimal relay selection for the parallel hybrid RF/FSO relay channel: Non-buffer-aided and buffer-aided designs," *IEEE Trans. Commun.*, vol. 65, no. 7, pp. 2794–2810, Jul. 2017.

[27] G. D. Roumelas, H. E. Nistazakis, E. Leitgeb, H. D. Ivanov, C. K. Volos, and G. S. Tombras, "Serially DF relayed hybrid FSO/MMW links with Weibull fading, M-turbulence and pointing errors," *Optik*, vol. 216, Aug. 2020, Art. no. 164531.

[28] O. Awwad, A. Al-Fuqaha, B. Khan, and G. B. Brahim, "Topology control schema for better QoS in hybrid RF/FSO mesh networks," *IEEE Trans. Commun.*, vol. 60, no. 5, pp. 1398–1406, May 2012.

[29] M. Abramowitz and I. A. Stegun, *Handbook of Mathematical Functions*. New York, NY, USA: Dover, 1965.

[30] M. K. Simon and M.-S. Alouini, *Digital Communication Over Fading Channels*, 2nd ed. New York, NY, USA: Wiley-IEEE Press, 2005.

[31] M. Mokhtar, N. Al-Dhahir, and R. Hamila, "OFDM full-duplex DF relaying under I/Q imbalance and loopback self-interference," *IEEE Trans. Veh. Technol.*, vol. 65, no. 8, pp. 6737–6741, Aug. 2016.

[32] H. AlQuwaiee, H.-C. Yang, and M.-S. Alouini, "On the asymptotic capacity of dual-aperture FSO systems with generalized pointing error model," *IEEE Trans. Wireless Commun.*, vol. 15, no. 9, pp. 6502–6512, Sep. 2016.

[33] F. Yang, J. Cheng, and T. A. Tsiftsis, "Free-space optical communication with nonzero boresight pointing errors," *IEEE Trans. Commun.*, vol. 62, no. 2, pp. 713–725, Feb. 2014.

[34] J. Zhang, L. Dai, Y. Han, Y. Zhang, and Z. Wang, "On the ergodic capacity of MIMO free-space optical systems over turbulence channels," *IEEE J. Sel. Areas Commun.*, vol. 33, no. 9, pp. 1925–1934, Sep. 2015.

[35] M. A. Al-Habash, L. C. Andrews, and R. L. Phillips, "Mathematical model for the irradiance probability density function of a laser beam propagating through turbulent media," *Opt. Eng.*, vol. 40, no. 8, pp. 1554–1562, Aug. 2001.

[36] M. C. Al Naboulsi, H. Sizun, and F. de Fornel, "Fog attenuation prediction for optical and infrared waves," *Opt. Eng.*, vol. 43, no. 2, p. 319, Feb. 2004.

[37] A. K. Majumdar, "Free-space laser communication performance in the atmospheric channel," *J. Opt. Fiber Commun. Rep.*, vol. 2, pp. 345–396, Nov. 2005.

[38] L. C. Andrews, R. L. Phillips, R. J. Sasiela, and R. Parenti, "Beam wander effects on the scintillation index of a focused beam," in *Proc. Atmospher. Propag. II*, vol. 5793, May 2005, pp. 28–37.

[39] K. Kiasaleh, "On the probability density function of signal intensity in free-space optical communications systems impaired by pointing jitter and turbulence," *Opt. Eng.*, vol. 33, no. 11, pp. 3748–3757, Nov. 1994.

[40] L. C. Andrews and R. L. Phillips, "Recent results on optical scintillation in the presence of beam wander," in *Proc. Atmospher. Propag. Electromagn. Waves II*, vol. 6878, Feb. 2008, pp. 23–36.

[41] T. Kwon, S. Lim, S. Choi, and D. Hong, "Optimal duplex mode for DF relay in terms of the outage probability," *IEEE Trans. Veh. Technol.*, vol. 59, no. 7, pp. 3628–3634, Sep. 2010.

[42] A. Leon-Garcia, *Probability, Statistics, and Random Processes For Electrical Engineering*, 3rd ed. Upper Saddle River, NJ, USA: Pearson, 2008.

[43] B. Epstein, "Some applications of the Mellin transform in statistics," *Ann. Math. Stat.*, vol. 19, no. 3, pp. 370–379, Sep. 1948.

[44] I. S. Gradshteyn and I. M. Ryzhik, *Table of Integrals, Series, and Products*, 7th ed. Burlington, MA, USA: Elsevier, 2007.

[45] V. S. Adamchik and O. I. Marichev, "The algorithm for calculating integrals of hypergeometric type functions and its realization in REDUCE system," in *Proc. Int. Symp. Symbolic Algebraic Comput.*, Tokyo, Japan, 1990, pp. 212–224.

MICHALIS P. NINOS (Member, IEEE) received the B.Sc. degree in physics and the M.Sc. degree in applied physics from the University of Patras, Greece, in 2009 and 2012, respectively, and the Ph.D. degree in optical wireless communications from the National and Kapodistrian University of Athens, Greece, in 2019. From 2005 to 2010, he served as a member of the Board of Directors of a technical company in Greece, having participated in several large-scale technical projects. From September 2020, he was a Postdoctoral Research Associate with the IRIDA Research Centre for Communications Technologies, Department of Electrical and Computer Engineering, University of Cyprus. His research interests lie in the fields of information and communications technologies, optical wireless, radio and quantum communications, hybrid RF/FSO, microelectronics, and physics of semiconductors.

PRIYADARSHI MUKHERJEE (Member, IEEE) received the B.Tech. degree in electronics and communication engineering from the Kalyani Government Engineering College, West Bengal University of Technology, India, in 2012, the M.Engg. degree in electronics and telecommunication engineering from the Indian Institute of Engineering Science and Technology, Shibpur, in 2014, and the Ph.D. degree in electrical engineering from the Indian Institute of Technology Delhi, Delhi, in 2019. He is currently a Postdoctoral Research Fellow of the IRIDA Research Centre for Communication Technologies, Department of Electrical and Computer Engineering, University of Cyprus. His research interests include cross-layer energy-efficient 5G system design, wireless information and power transfer, and full-duplex communication.

CONSTANTINOS PSOMAS (Senior Member, IEEE) received the B.Sc. degree in computer science and mathematics from the Royal Holloway, University of London in 2007, the M.Sc. degree in applicable mathematics from the London School of Economics in 2011, and the Ph.D. degree in mathematics from The Open University, U.K., in 2011. He is currently a Research Fellow of the Department of Electrical and Computer Engineering, University of Cyprus. From 2011 to 2014, he was as a Postdoctoral Research Fellow of the Department of Electrical Engineering, Computer Engineering and Informatics, Cyprus University of Technology. His current research interests include wireless powered communications, cooperative networks, and full-duplex communications. He received an Exemplary Reviewer Certificate by the IEEE Transactions on Communications for 2020 and by the IEEE WIRELESS COMMUNICATIONS LETTERS for 2015 and 2018. He serves as an Associate Editor for the IEEE WIRELESS COMMUNICATIONS LETTERS and the *Frontiers in Communications and Networks*.

IOANNIS KRIKIDIS (Fellow, IEEE) received the Diploma degree in computer engineering from the Computer Engineering and Informatics Department, University of Patras, Greece, in 2000, and the M.Sc. and Ph.D. degrees in electrical engineering from the École Nationale Supérieure des Télécommunications (ENST), Paris, France, in 2001 and 2005, respectively.

From 2006 to 2007, he worked as a Postdoctoral Researcher with ENST and from 2007 to 2010 he was a Research Fellow of the School of Engineering and Electronics, The University of Edinburgh, Edinburgh, U.K. He is currently an Associate Professor with the Department of Electrical and Computer Engineering, University of Cyprus, Nicosia, Cyprus. His current research interests include wireless communications, cooperative networks, 5G communication systems, wireless powered communications, and secrecy communications. He was a recipient of the Young Researcher Award from the Research Promotion Foundation, Cyprus, in 2013, the IEEE ComSoc Best Young Professional Award in Academia, 2016, and IEEE SIGNAL PROCESSING LETTERS Best Paper Award 2019. He has received the prestigious ERC Consolidator Grant. He has been recognized by the Web of Science as a Highly Cited Researcher form 2017 to 2020. He serves as an Associate Editor for IEEE TRANSACTIONS ON WIRELESS COMMUNICATIONS, IEEE TRANSACTIONS ON GREEN COMMUNICATIONS AND NETWORKING, and IEEE WIRELESS COMMUNICATIONS LETTERS. He is also a Founding Specialty Chief Editor for Communication Theory in *Frontiers Communications and Networks*.